NANOSYSTEMS: PHYSICS, CHEMISTRY, MATHEMATICS, 2014, 5 (6), P. 854–860

NANOCRYSTALLINE PEROVSKITE-LIKE OXIDES FORMATION IN $Ln_2O_3 - Fe_2O_3 - H_2O$ (Ln = La, Gd) SYSTEMS

E. A. Tugova, O. N. Karpov

Ioffe Physical Technical Institute of RAS, Saint Petersburg, Russia

katugova@inbox.ru

PACS 61.46.-w; 82.80.Ej

Nanocrystalline $LnFeO_3$ (Ln = La, Gd) ferrites have been prepared by the co-precipitation method followed by heat treatment in air. The formation mechanisms for $LaFeO_3$ and $GdFeO_3$ in $Ln_2O_3 - Fe_2O_3 - H_2O$ (Ln = La, Gd) systems under the mentioned conditions are investigated. The phase interaction scheme, reflecting ways which lead to the target, synthesis product yield, as well as the common tendency of $LaFeO_3$ and $GdFeO_3$ formation mechanisms, are constructed. The mean sizes of coherent scattering regions of $LaFeO_3$ and $GdFeO_3$ were determined to be 30±3 and 40±4 nm, respectively.

Keywords: $LnFeO_3$, ferrites, nanostructures, precipitation technique, phase formation, X-Ray diffraction.

Received: 5 November 2014

Revised: 27 November 2014

1. Introduction

Perovskite-like oxides, produced by different synthetic methods and having a variety of structural peculiarities, possess a complex array of electric, magnetic, catalytic, thermal, and other properties being of interest, in terms of practical applications [1-20]. Conventionally, the most common technique for obtaining complex oxides, including perovskite-like phases, is the method of solid-state synthesis [21-23]. Usually, for solid-state synthesis, simple oxides, carbonates, nitrates, oxalates, citrates or other salts of proper metals can be used as reagents. To ensure stoichiometry of the compounds synthesized, definite composition of gaseous medium can be prescribed, i.e. air, nitrogen, oxygen, hydrogen, etc. Despite a great number of papers devoted to the solid-state synthesis of perovskite-like oxides and to research into the peculiarities of their structure and properties [12, 17-21], limited data on the formation processes for perovskite-like oxides are available. There is also insufficient data on state equilibria for $Ln_2O_3 - Fe_2O_3$ (Ln = La, Gd) systems, which include perovskite-like oxides. Additionally, since the composition of the substances determines their basic properties, the lack of the mentioned data may affect the preparation of materials based on perovskite-like oxides with function-oriented characteristics.

Recently, the preparation of perovskite-like oxides using "soft chemistry" techniques has become of greater interest [24-25]. This is determined by the practical application of nanomaterials with unique structure and properties prepared using "soft chemistry" techniques [26]. However, mechanisms for the formation of the considered compounds remain mostly unstudied, which is associated, inter alia, with a lack of reliable generalized data on stability regions, processes of decomposition of intermediate substances, typically, *p*-, *d*- and *f*-elements hydroxides resulting from the reactions of precipitation, hydrolysis, etc., i.e. those proceeding, primarily, in aqueous media. Shafer and Roy attempted to determine stability of

rare-earth oxides and hydroxides in studying the state equilibria of Ln_2O_3 – H_2O (Ln= La, Nd, Sm) systems [27]. Lanthanum oxide was found to differ from neodymium and samarium, primarily, in its greater tendency towards hydration. The authors were not able to determine whether LaOOH monohydrate or La_2O_3 forms via the decomposition of lanthanum hydroxide, or its crystal structure. The authors of [28] studied the dehydration kinetics for $Gd(OH)_3$ obtained via hydrothermal conditions. The chemical transformations within the Fe_2O_3 – H_2O system within media of different pH and with different P-T-conditions were investigated in [29, 30]. Papers [2, 5, 31] also discussed the formation of $LaFeO_3$ during the dehydration of components of the La_2O_3 – Fe_2O_3 – H_2O system. It has been reported that for the preparation of $GdFeO_3$ nanoparticles using polyol technique, the authors obtained an until-then unknown compound corresponding to the formula Gd_3FeO_6, extending the number of compounds formed in the Gd_2O_3-Fe_2O_3-H_2O system [32].

Thus, in literature, there are a number of works concerning the study of nanocrystalline perovskite-like oxides using "soft chemistry" techniques. However, to describe the mechanisms of perovskite-like oxides formation using "soft chemistry" techniques requires application of a comprehensive approach, taking into account information about phase equilibria in the systems where perovskite-like oxides could form, and analysis of the impact chemical background could have on the formation of the synthetic targets.

Therefore, the data investigation aims at studying of the formation processes of nanoscale perovskite-like oxides in Ln_2O_3 – Fe_2O_3 – H_2O (Ln = La, Gd) systems differing in synthetic prehistory.

2. Experimental

2.1. Synthesis procedure

$LnFeO_3$ (Ln = La, Gd) samples were prepared the by precipitation method from aqueous solutions of stoichiometric amounts of 1M $Ln(NO_3)_3{\cdot}6H_2O$ and $Fe(NO_3)_3{\cdot}9H_2O$. Aqueous 10 wt.% NH_4OH was used as the precipitating medium. To the NH_4OH medium, the aqueous solutions of lanthanum, gadolinium and iron nitrates were added in a dropwise manner by adjusting the pH value to 8–9. The co-precipitated mixtures were filtered immediately after preparation to remove traces of NO_3^- ions. Samples were then dried at room temperature in air. These initial mixtures were then pressed and calcined in air at 500–900°C for 3 h.

2.2. Characterization of prepared nanocrystalline perovskite-related oxides

The purity and crystal structure of $LnFeO_3$ (Ln = La, Gd) samples were characterized by powder X-ray diffraction (XRD) using Shimadzu XRD-7000 with monochromatic CuK_α radiation (λ= 154.178 pm). α-Al_2O_3 was used as an internal standard. Crystallite sizes of the obtained powders were calculated by the X-ray line broadening technique based on Scherer's formula.

The elemental composition and the composition of separate phases were analyzed by means of scanning electron microscopy (SEM) using Quanta 200, coupled with EDAX microprobe analyzer. The error in determining the elements content by this method varies with the atomic number and equals to 0.3 mass% on average.

The IR spectroscopic investigations of samples were carried out on an FSM-1202 Fourier-transform spectrometer from 400–4000 cm^{-1}. Samples were prepared as KBr pellets.

3. Results and discussion

X-ray phase analysis of precipitated mixtures testifies to their X-ray amorphous condition. Elemental analysis showed that the stoichiometric ratio of Ln:Fe is 1.00:1.06, which is close to that of the synthetic targets, $LnFeO_3$ (Ln = La, Gd). Furthermore, the obtained samples were exposed to thermal treatment from 500 to 900° in air (p_{O_2} = 0.21 atm.).

Fig. 1*a* shows the data obtained from X-ray phase analysis for samples corresponding to the stoichiometry of $LaFeO_3$ after thermal treatment from 500 to 900°C in air. According to the X-ray phase analysis, when the initial mixture was exposed to thermal treatment at 500°C for 3 hours, $La_2O_2CO_3$ is crystallized as a monoclinic structure. The IR spectrometric analysis of this sample showed presence of bandwidths at 3,650-3,300; 2,936; 2,862; 1,774; 1,639; 1,500; 1,450-1,400; 1,388; 1,057-1,076; 856-900; 700-725 cm^{-1} (see table), which can be attributed to valence and deformation vibrations of crystallization water, Fe-O groups typically found in $Fe(OH)_3$, Fe_2O_3, $La_2O_2CO_3$ (Fig. 1*b*) spectra. Raising the initial mixture processing temperature to 600°C will lead to a decrease in the bandwidth intensity, associated with the removal of crystallization water (3,500–3,200; 1,630 cm^{-1}), and with initiation of decarbonation of $La_2O_2CO_3$, forming La_2O_3. According to the data presented (see Fig. 1, table) the reaction mixture thermally treated at 600 and 900°C contained a wide bandwidth at frequency 670–530 cm^{-1}, which can be referred to as a band corresponding to La-O-Fe vibrations in perovskite structure, by analogy with [33, 34]. The data obtained agree with the results of X-ray phase analysis for samples exposed to thermal processing at 600°C when the formation of $LaFeO_3$ is recorded. The size of the regions of coherent scattering for $LaFeO_3$, prepared by thermal treatment of the co-precipitated mixture at 600°C, was 30±3 nm.

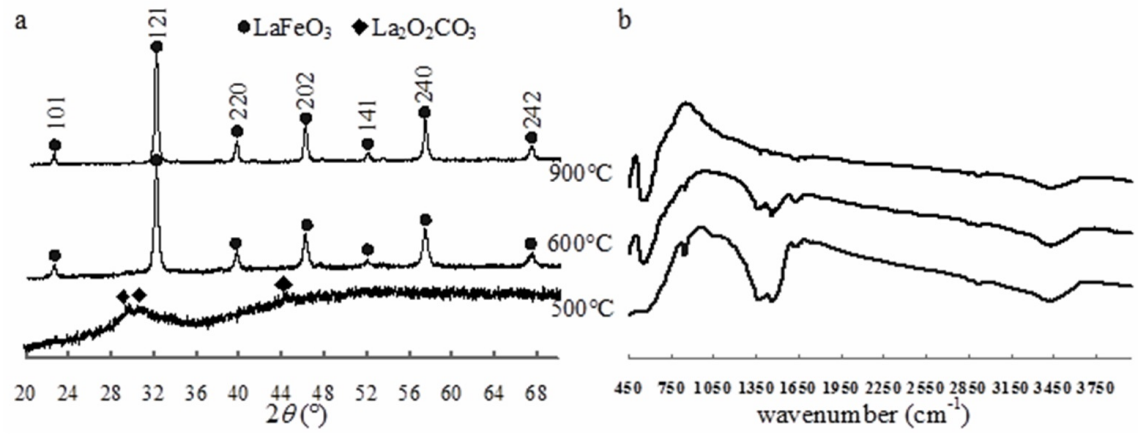

Fig. 1.) X-Ray diffraction patterns and b) IR transmission spectra of initial mixture corresponding with stoichiometry of $LaFeO_3$ heat treated in the air

Thus, the activation temperature for the formation of $LaFeO_3$ is connected with the decarbonation of $La_2O_2CO_3$, proceeding from 500 – 600°C, with La_2O_3 thus formed, initiating the generation of nanoscale perovskite-like lanthanum ferrite from 600°C.

Fig. 2 shows the X-ray phase analysis for samples corresponding to a stoichiometry of $GdFeO_3$, prepared after thermal treatment of the initial mixture from 500 to 900°C in air. According to the presented X-ray phase analysis data (Fig. 2), the samples thermally treated from 500 to 600°C contain Gd_2O_3 and $Gd_2O_2CO_3$ phases. The appearance of $Gd_2O_2CO_3$ in the reaction mixture may be caused by utilizing synthetic precursors that were previously

TABLE. IR spectroscopic data of the initial mixture on stoichiometry closed to $LaFeO_3$, heat treated at 500, 600, 900°C temperatures versus reference data [33-34]

Experimental data			Reference data [33-34]				
wavenumber (cm^{-1})			wavenumber (cm^{-1})				
500°C	600°C	900°C	H_2O	$La_2O_2CO_3$	$La(OH)_3$	$Fe(OH)_3$	α-Fe_2O_3
515-670	530-670	530-670	650	660-680-730	655		500-620
858	860-875			860-870-880			
1075	1080			1050-1060-1080		1080	
1382	1375	1388		1380		1353	1388
1473	1468-1500			1470-1500		1500	
1638	1645	1650	1600-1630			1634	1656
2862	2859	2859					2865
2928	2934	2934	2930				2951
3350-3600	3350-3600	3400-3600	3200-3550		3420, 3600		

dried in air (and thus exposed to CO_2). According to [35], $Gd_2O_2CO_3$ exists in layered structures consisting of alternating $(Ln_2O_2^{2+})_n$ and carbonate groups $(CO_3)_n^{2n-}$ layers. Raising the thermal treatment temperature will result in decarbonation, leading to the formation of cubic crystallized active-reactive Gd_2O_3. According to [35], $Gd_2O_2CO_3$ decomposes as follows: $Gd_2O_2CO_3 \xrightarrow{650°C} Gd_2O_3 + \uparrow CO_2$. According to the presented data of X-ray phase analysis (Fig. 2), starting from 700°C, the $GdFeO_3$ phase is formed. The mean size of coherent scattering regions, calculated from reflex with 111 index for the $GdFeO_3$ sample obtained after thermal treatment of the initial mixture at 700°C, was 40±4 nm.

Thus, the activation temperature for the formation of $GdFeO_3$, in the case when one of the reagents is $Gd_2O_2CO_3$, shall be determined by its decarbonation temperature at 600–700°C, leading to the formation of active-reactive Gd_2O_3. In such a case, the formation of nanoscale perovskite-like gadolinium ferrite will be recorded as starting from 700°C.

Thus, in case when initial compositions were obtained by the co-precipitation method, the processes for $LnFeO_3$ nanoparticle formation can be represented as a scheme depicted in Fig. 3, exemplified by the formation of $GdFeO_3$ nanocrystals. The diagram is given with experimental and literature data [27-30, 33-35] taken into consideration. The formation of FeO(OH) and $Gd(OH)_3$ hydroxides, mixed on the molecular level at the initial stages of synthesis, apparently, may lead to the formation of $GdFeO_3$ nanoparticles, with simultaneous dehydration of both components. The second mechanism is connected with both dehydration and decarbonation processes, the latter proceeding at a higher temperature. In connection with this, localized in space Fe_2O_3 and Gd_2O_3 will interact at the next stage. This will lead to a rise in the synthesis temperature for $GdFeO_3$ and to an increase in the size of the formed crystals. The obtained results correlate with the previous conclusions [22]. Note that if $GdFeO_3$ nanocrystals are prepared via hydrothermal methods, the initial mixture obtained according to the technique described in this paper, we also record a difference in the nature of intermediate products, despite carrying out the synthesis in an aqueous medium [1].

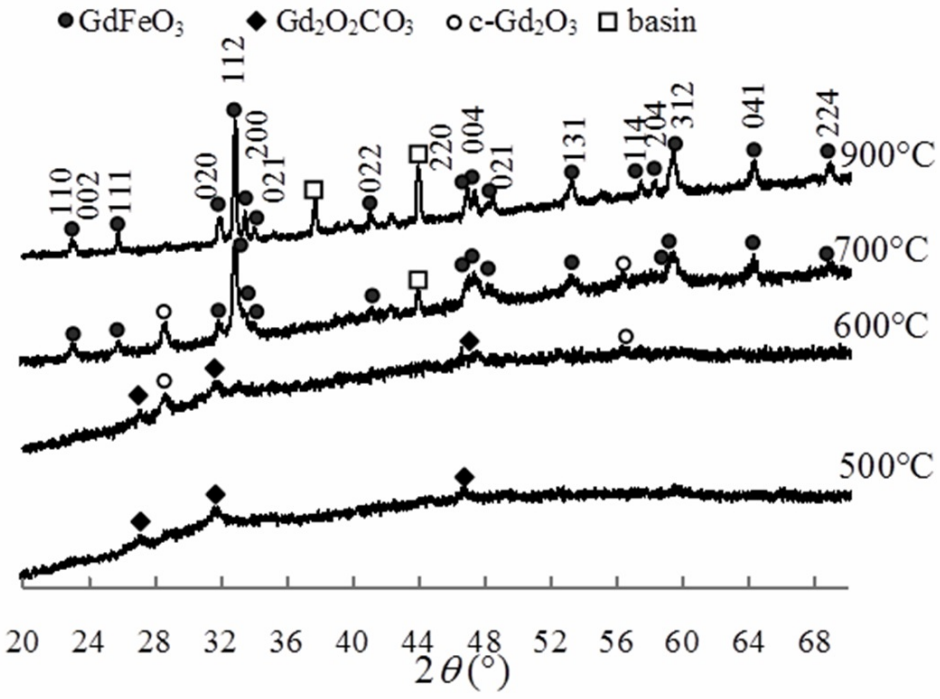

Fig. 2. X-Ray diffraction patterns of initial mixtures corresponding with stoichiometry of $GdFeO_3$ after sintering within the temperature range 500 to 900°C in the air

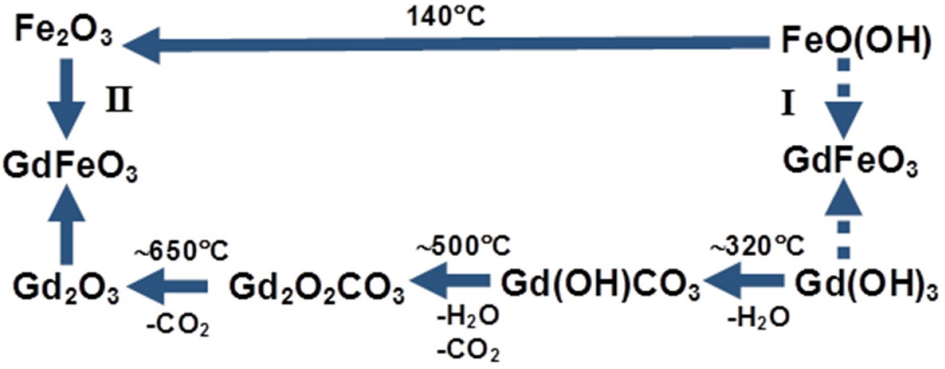

Fig. 3. $LnFeO_3$ nanocrystals formation scheme exemplified by the forming of $GdFeO_3$ under the heat treatment of co-precipitated initial mixture in air Remarks: I - the mechanism of co-precipitated hydroxides simultaneous dehydration with $GdFeO_3$ formation; II - the scheme of step-by-step transformations of co-precipitated components with spatial-isolated Fe_2O_3 and Gd_2O_3 nanoparticles formation followed by solid state interaction for $GdFeO_3$ production

4. Conclusion

Therefore, the mechanism for perovskite-related lanthanum and gadolinium ferrites formation depends heavily on chemical processes resulting in the spatial separation of components of a target product. In particular, these processes may determine the temperature at which perovskite-related ferrite begins to form, as well as the size of the formed nanocrystals.

Acknowledgments

The authors would like to thank Prof. V.V. Gusarov very much for useful discussions and valuable advice.

References

[1] Tugova E.A., Zvereva I.A. Formation mechanism of $GdFeO_3$ nanoparticles under the hydrothermal conditions. *Nanosystems: physics, chemistry, mathematics*, **4**(6), P. 851–856 (2013).

[2] Nakayama S. $LaFeO_3$ perovskite type oxide prepared by oxide mixing co-precipitation and complex synthesis methods. *J. Mater. Sci.*, **6**, P. 5643–5648 (2001).

[3] Tang P., Chen H., Cao F., Pan G. Magnetically recoverable and visible light driven nanocrystalline $YFeO_3$ photocatalysts. *Catal. Sci. Technol.*, **1**(7), P. 1145–1148 (2011).

[4] Nguyen A.T., Mittova I.Ya., Al'myasheva O.V. Influence of the synthesis conditions on the particle size and morphology of yttrium orthoferrite obtained from aqueous solutions. *Russ. J. Appl. Chem.*, **82**(11), P. 1915–1918 (2009).

[5] Nguyen A.T., Mittova I.Ya., Almjasheva O.V., Kirillova S.A., Gusarov V.V. Influence of the preparation conditions on the size and morphology of nanocrystalline lanthanum orthoferrite. *Glas. Phys. Chem.*, **34**(6), P. 756–761 (2008).

[6] Shang M., Zhang C., Zhang T., Yuan L., Ge L. Yuan H., Feng S. The multiferroic perovskite $YFeO_3$. *Appl. Phys. Lett.*, **102**(6), 062903(3 pages) (2013).

[7] Zhou Z., Guo L., Yang H., Liu Q., Ye F. Hydrothermal synthesis and magnetic properties of multiferroic rare-earth orthoferrites. *J. Alloys Compd*, **583**, P. 21–31 (2014).

[8] Tang P., Sun H., Chen H., Cao F. Hydrothermal processing-assisted synthesis of nanocrystalline $YFeO_3$ and its visible-light photocatalytic activity. *Curr. Nanosci.*, **8**, P. 64–67 (2012).

[9] Nguyen A.T., Almjasheva O.V., Mittova I.Ya., Stognei O.V., Soldatenko S.A. Synthesis and magnetic properties of $YFeO_3$ nanocrystals. *Inorganic Materials*, **45**(11), P. 1304–1308 (2009).

[10] Zhang Yu., Yang J., Xu J., Gao Q., Hong Zh. Controllable synthesis of hexagonal and orthorhombic $YFeO_3$ and their visible-light photocatalytic activities. *Materials Letters*, **81**, P. 1–4 (2012).

[11] Maiti R., Basu S., Chakravorty D. Synthesis of nanocrystalline $YFeO_3$ and its magnetic properties. *Journal of Magnetism and Magnetic Materials*, **321**(19), P. 3274–3277 (2009).

[12] Venugopalan A., Appasamy M., Saravanan S., Kothandaraman K., Kothandaraman J. Structural, electrical and magnetic studies on Y-Fe-O system. *Journal of Rare Earths*, **27**(6), P. 1013–1017 (2009).

[13] Lu X., Xie J., Shu H., Liu J., Yin Ch., Lin J. Microwave-assisted synthesis of nanocrystalline $YFeO_3$ and study of its photoactivity. *Materials Science and Engineering B*, **138**, P. 289–292 (2007).

[14] Zhang W., Fang C.X, Yin W.H, Zeng Y.W. One-step synthesis of yttrium orthoferrite nanocrystals via sol-gel auto-combustion and their structural and magnetic characteristics. *Mater. Chem. Phys.*, **137**(3), P. 877–883 (2013).

[15] Popkov V.I., Almjasheva O.V. Yttrium orthoferrite $YFeO_3$ nanopowders formation under glycine-nitrate combustion conditions. *Russian Journal of Applied Chemistry*, **87**(2), P. 167–171 (2014).

[16] Goswami S., Bhattacharya D., Choudhury P. Particle size dependence on magnetization and noncentrosymmetry in nanoscale $BiFeO_3$. *Journal of applied physics D*, **109**(7), P. 737–739 (2011).

[17] Egorysheva A.V., Volodin V.D., Ellert O.G., Efimov N.N., Skorikov V.M., Baranchikov A.E., Novotortsev V.M. Mechanochemical activation of starting oxide mixtures for solid-state synthesis of $BiFeO_3$. *Inorganic Materials*, **49**(3), P. 303–309 (2013).

[18] Morozov M. I., Lomanova N. A., Gusarov V.V. Specific features of $BiFeO_3$ formation in a mixture of bismuth (III) and iron (III) oxides. *Russ. J. Gen. Chem.*, **73**(11), P. 1772–1776 (2003).

[19] Lomanova N.A., Gusarov V.V. Effect of surface melting on the formation and growth of nanocrystals in the Bi_2O_3-Fe_2O_3 system. *Russ. J. Gen. Chem.*, **83**(12), P. 2251–2253 (2013).

[20] Lomanova N.A., Gusarov V.V. Influence of synthesis temperature on $BiFeO_3$ nanoparticles formation. *Nanosystems: physics, chemistry, mathematics*, **4**(5), P. 696–705 (2013).
[21] Tretyakov Yu. D., Lukashin A.V., Eliseev A. A. Synthesis of functional nanocomposites based on solid-phase nanoreactors. *Russian Chemical Reviews*, **73**(9), P. 899–923 (2004).
[22] Gusarov V.V. Fast solid-phase chemical reactions. *Russian Journal of General Chemistry*, **67**(12), P. 1846–1851 (1997).
[23] Schaak R.E., Mallouk Th. E. Perovskites by design: A toolbox of solid-state reactions. *Chemistry of Materials*, **14**, P. 1455–1471 (2002).
[24] Livage J. Vanadium pentoxide gels. *Chemistry of Materials*, **3**(4), P. 578–593 (1991).
[25] Sanchez C., Rozes L., Ribot F., Laberty-Robert C., Grosso D., Sassoye C., Boissiere C., Nicole L. "Chimie douce": A land of opportunities for the designed construction of functional inorganic and hybrid organic-inorganic nanomaterials. *Comptes Rendus Chimie*, **13**(1-2), P. 3–39 (2010).
[26] Gopalakrishnan J. Chimie. Douce approaches to the synthesis of metastable oxide materials. *Chemistry of Materials*, **7**(7), P. 1265–1275 (1995).
[27] Shafer M.W., Roy R. Rare-earth polymorphism and phase equilibria in rare-earth oxide-water systems. *Journal of the American Ceramic Society*, **42**(4), P. 563–570 (1959).
[28] Chang Ch, Mao D. Thermal dehydration kinetics of a rare earth hydroxide $Gd(OH)_3$. *International Journal of Chemical Kinetics*, **39**(2), P. 75–81. (2007)
[29] Tareen J.A.K., Krishnamurthy K.V. Hydrothermal stability of hematite and magnetite. *Bulletin Materials Science*, **3**(1), P. 9–13 (1981).
[30] Popov, V.V., Gorbunov, A.I. Hydrothermal Crystallization of iron (III) hydroxide. *Inorg. Materials*, **42**(3), P. 275–281 (2006).
[31] Xu H., Hu X., Zhang L. Generalized low-temperature synthesis of nanocrystalline rare earth orthoferrites $LnFeO_3$ (Ln=La, Pr, Nd, Sm, Eu, Gd). *Cryst. Growth Des.*, **8**(7), P. 2061–2065 (2008).
[32] Söderlind S., Fortin M.A, Petoral Jr R.M., Klasson A., Veres T., Engström M., Uvdal K., Käll P.-O. Colloidal synthesis and characterization of ultrasmall perovskite $GdFeO_3$ nanocrystals. *Nanotechnology*, **19**(8), P. 085608-(8pp) (2008).
[33] Tugova E.A. A comparative analysis of the formation processes of Ruddlesden-Popper phases in the La_2O_3-SrO-M_2O_3 (M = Al, Fe) systems. *Glas. Phys. Chem*, **35**(4), P. 416–422 (2009).
[34] Bernal S., Blanco G., Gatica J.M., Perez-Omil J.A., Pintado J.M., Vidal H. Chemical reactivity of binary rare earth oxides. Binary Rare Earth Oxides, Kluwer Academic Publishers, P. 9–55 (2004).
[35] Sheu H. Sh., Shih W.-J., Chuang W.-T., Li I.-F., Yeh Ch.-Sh. Crystal structure and phase transitions of $Gd(CO_3)OH$ studied by synchrotron powder diffraction. *Journal of the Chinese Chemical Society*, **57**(4), P. 938–945 (2010).